

ESD ACCESSION LIST

XRRI Call No.

83712

Copy No.

1 of 2 cys.

FILE COPY

Semiannual Technical Summary

Integrated Optical Circuits

31 December 1974

Prepared for the Advanced Research Projects Agency
under Electronic Systems Division Contract F19628-73-C-0002 by

Lincoln Laboratory

MASSACHUSETTS INSTITUTE OF TECHNOLOGY

LEXINGTON, MASSACHUSETTS



Approved for public release; distribution unlimited.

ADA04254

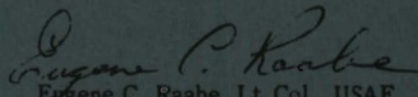
The work reported in this document was performed at Lincoln Laboratory, a center for research operated by Massachusetts Institute of Technology. This work was sponsored by the Advanced Research Projects Agency of the Department of Defense under Air Force Contract F19628-73-C-0002 (ARPA Order 2074) and is being monitored by Air Force Cambridge Research Laboratories.

This report may be reproduced to satisfy needs of U.S. Government agencies.

The views and conclusions contained in this document are those of the contractor and should not be interpreted as necessarily representing the official policies, either expressed or implied, of the Defense Advanced Research Projects Agency of the United States Government.

This technical report has been reviewed and is approved for publication.

FOR THE COMMANDER



Eugene C. Raabe, Lt. Col., USAF
Chief, ESD Lincoln Laboratory Project Office

Non-Lincoln Recipients

PLEASE DO NOT RETURN

Permission is given to destroy this document
when it is no longer needed.

MASSACHUSETTS INSTITUTE OF TECHNOLOGY
LINCOLN LABORATORY

INTEGRATED OPTICAL CIRCUITS

SEMIANNUAL TECHNICAL SUMMARY REPORT
TO THE
ADVANCED RESEARCH PROJECTS AGENCY

1 JULY - 31 DECEMBER 1974

ISSUED 23 JULY 1975

Approved for public release; distribution unlimited.

LEXINGTON

MASSACHUSETTS

ABSTRACT

Detailed measurements of the attenuation of high-purity planar GaAs waveguides have been made over the wavelength range from 0.90 to 1.06 μm . The loss, which appears to be primarily due to a band-edge absorption tail, ranges from 3.0 cm^{-1} at 0.90 μm to 0.3 cm^{-1} at 1.06 μm and is $\leq 1\text{ cm}^{-1}$ for $\lambda > 0.909\text{ }\mu\text{m}$. These waveguides are suitable for use with Si-doped GaAs-AlGaAs integrated lasers and with integrated electroabsorption detectors and modulators.

Integrated structures consisting of Fabry-Perot GaAs-AlGaAs double-heterostructure lasers immersed in high-purity GaAs slab waveguides have been fabricated and characterized. These structures are quite attractive for use as sources in GaAs-based monolithic integrated optical circuits. Threshold current densities at room temperature as low as 7.5 kA/cm^2 for 1- μm -thick active regions were measured. Measured external differential quantum efficiencies of the laser-waveguide combinations were about 3.5 percent, but appeared to be limited by the presence of internally circulating modes.

Over three-orders-of-magnitude reduction of lattice-misfit dislocation densities in heteroepitaxial $\text{Pb}_{0.88}\text{Sn}_{0.12}\text{Te}$ layers grown either by molecular beam or liquid-phase epitaxy has been achieved by growing the layers on nearly lattice-matched $\text{PbTe}_{0.952}\text{Se}_{0.048}$ substrates. The etch-pit density of the layers is in the range of 10^4 cm^{-2} , and is comparable to that of the substrates.

CONTENTS

Abstract	iii
I. GaAs-Based Integrated Optical Circuits	1
A. Low-Loss High-Purity GaAs Waveguides	1
B. Integrated GaAs-AlGaAs Double-Heterostructure Lasers	3
II. Lead-Salt Integrated Optical Circuits: Lattice-Misfit Dislocations in Heteroepitaxial $\text{Pb}_{1-x}\text{Sn}_x\text{Te}$	7
References	9

INTEGRATED OPTICAL CIRCUITS

I. GaAs-BASED INTEGRATED OPTICAL CIRCUITS

A. LOW-LOSS HIGH-PURITY GaAs WAVEGUIDES

GaAs has been extensively investigated as a material for integrated optical circuit light guides at 1.06- and 1.15- μm wavelengths. Low-loss, three-dimensional waveguides of several different types have been fabricated.^{1,2} The change in refractive index which is responsible for the guiding action in these structures has been obtained by using either heavily doped substrate material (and in some instances also a heavily doped cladding material) which has a lower index of refraction, or a wider-bandgap material such as $\text{Al}_x\text{Ga}_{1-x}\text{As}$ which also has a lower refractive index, as the cladding for the GaAs waveguides. Losses as low as 2 cm^{-1} also have been achieved at these wavelengths with three-dimensional waveguides formed by using proton bombardment to decrease the carrier concentration.³ However, because the GaAs material used in all these waveguides was relatively heavily doped or compensated, the absorption tails close to the band edge made these guides extremely lossy at shorter wavelengths. These absorption tails presumably result from the Franz-Keldysh effect and internal electric fields which are due to ionized impurities or other defects.⁴ It should therefore be possible to reduce these losses by using high-purity GaAs for the waveguide material.

To investigate this possibility, we have made transmission measurements on planar high-purity GaAs light guides at wavelengths close to the band edge. These measurements indicate that low-loss guides ($\alpha \lesssim 1\text{ cm}^{-1}$) for use with GaAs room-temperature lasers can be fabricated in this material. Besides simplifying the fabrication procedures for integrated optical circuits, these waveguides are well suited to the incorporation of electroabsorption modulators and detectors.

A schematic diagram of the arrangement used to measure the waveguide transmission is shown in Fig. 1. The source is a grating-controlled external cavity GaAs room-temperature laser.⁵ By adjusting the grating angle, the laser wavelength can be tuned over approximately a 150- \AA wavelength range in the vicinity of about 0.9 μm . A series of about five different laser diodes permits the entire wavelength range between about 0.93 and 0.85 μm or less to be covered.

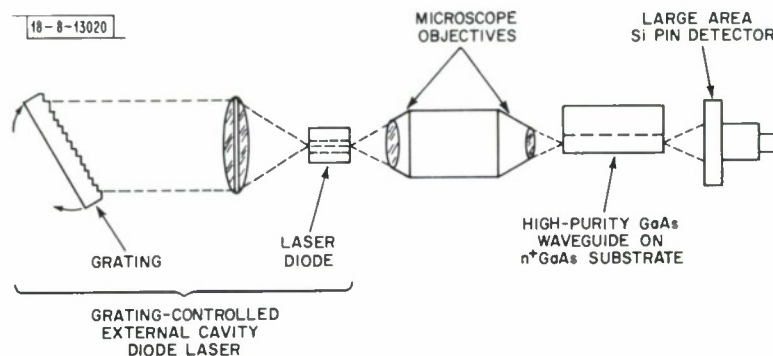


Fig. 1. Schematic diagram of experimental arrangement used to measure the loss coefficient of high-purity GaAs waveguides.

The emission from the laser was collimated by a microscope objective and then either directed to a spectrometer for wavelength calibration, or focused on a cleaved edge of the planar waveguides for the transmission measurements. The emission from the other cleaved edge of the planar waveguides was observed with an infrared microscope for alignment purposes. For quantitative transmission measurements, the incident laser power, as well as the power emitted from the cleaved edge of the waveguide, was measured using a large area Si PIN detector. By making the transmission measurements on two or more different lengths of guides, the exponential loss coefficient of the planar waveguides could be calculated.

The variation of the exponential loss coefficient with wavelength for one planar high-purity GaAs waveguide is shown in Fig. 2. The epitaxial material for this waveguide was unintentionally

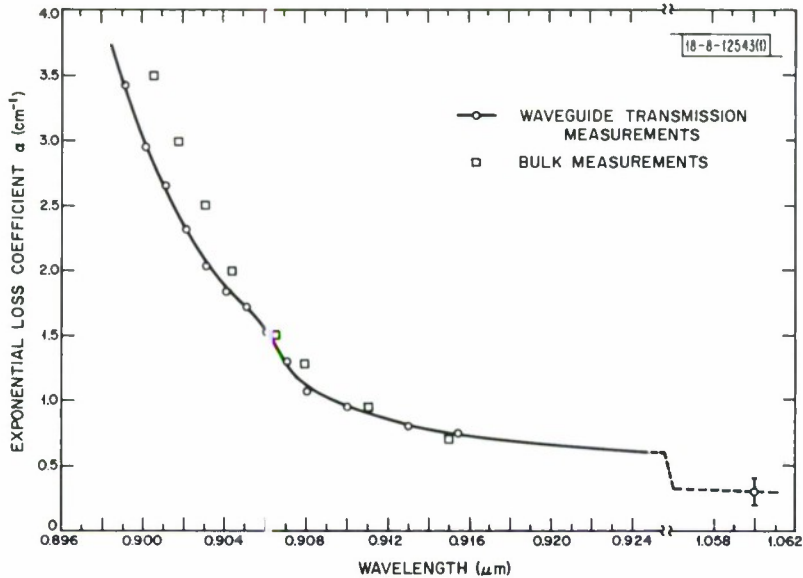


Fig. 2. Experimental loss coefficient for a high-purity GaAs waveguide (circles) and for a bulk sample of comparable purity (squares).

doped, compensated high-resistivity GaAs with a total ionized impurity concentration estimated to be in the low 10^{14}-cm^{-3} range. The free-carrier concentration of the 20- μm -thick epitaxial layer was $\lesssim 10^{12}\text{ cm}^{-3}$ and the substrate-carrier concentration was $1 \times 10^{18}\text{ cm}^{-3}$, which gives a refractive index difference between the layers of 1.4×10^{-3} . For these guide parameters, a total of five modes could propagate. The exponential loss coefficients shown were calculated from transmission measurements on three different waveguides of 1.4-, 0.9-, and 0.5-cm lengths. The error bars on the point at 1.06 μm indicate the uncertainty in the loss coefficient α from the three different measurements. There is a gradual increase in α from 0.3 cm^{-1} at 1.06 μm to 0.7 cm^{-1} at 0.915 μm . For shorter wavelengths, the increase is more rapid, reaching 0.95 cm^{-1} at 0.910 μm and 1.5 cm^{-1} at 0.905 μm . The more rapid increase in the loss at the shorter wavelengths is due to the nearness of the absorption edge. As mentioned earlier, the absorption at these wavelengths is presumably due to the Franz-Keldysh effect in conjunction with the internal electric fields in the crystal which result from ionized impurities or other crystal defects. The small shoulder present at 0.905 μm has been observed previously in other

absorption and photoconductive measurements, but its origin has not been determined. Also shown in this figure (by the square data points) is the wavelength variation of the absorption coefficient determined from measurements on bulk material (epitaxial layers with the substrate removed) with a total ionized impurity concentration of $5 \times 10^{14} \text{ cm}^{-3}$ and a liquid nitrogen temperature mobility of $160,000 \text{ cm}^2/\text{V}\cdot\text{sec}$. This material was selected because its purity was comparable to that estimated for the waveguide material. The slightly higher measured loss for the bulk material indicates that the total ionized impurity content for this material is slightly higher than that of the waveguide, since the losses for the guided radiation would be higher than the bulk absorption on the same material because of the effects of higher-order modes, scattering, etc.

G. E. Stillman
 C. M. Wolfe
 J. A. Rossi

B. INTEGRATED GaAs-AlGaAs DOUBLE-HETEROSTRUCTURE LASERS

The capability of integrating a laser source with a passive optical waveguide is an important element in the fabrication of a monolithic integrated optical circuit. One such structure, which utilizes the "twin guide" concept whereby light from a GaAs-AlGaAs laser is coupled downward into an AlGaAs waveguide parallel to the laser active region, has been demonstrated by Suematsu *et al.*⁶ Reinhart and Logan⁷ also have described a different structure wherein a passive AlGaAs waveguide layer has been included within the Fabry-Perot cavity of a GaAs-AlGaAs laser.

Another approach, which we have successfully implemented, involves the integration of an independent Fabry-Perot GaAs-AlGaAs double-heterostructure (DH) laser with a high-purity GaAs passive waveguide. This structure has the features that it is planar, the fabrication and operation of the laser are completely independent of the waveguide, and it is compatible with Fabry-Perot, distributed feedback (DFB),⁸ or distributed Bragg reflector (DBR)⁹ lasers. Furthermore, it utilizes the low-loss ($\alpha \leq 1 \text{ cm}^{-1}$ at $\lambda = 9100 \text{ \AA}$) high-purity waveguides¹⁰ in which integrated electroabsorption modulators¹⁰⁻¹² and both electroabsorption¹³ and InGaAs avalanche detectors¹⁴ have been demonstrated.

A schematic cross section of the laser-waveguide structure is shown in Fig. 3. Fabrication of the devices began with a typical GaAs-AlGaAs DH wafer grown by liquid-phase epitaxy (LPE)

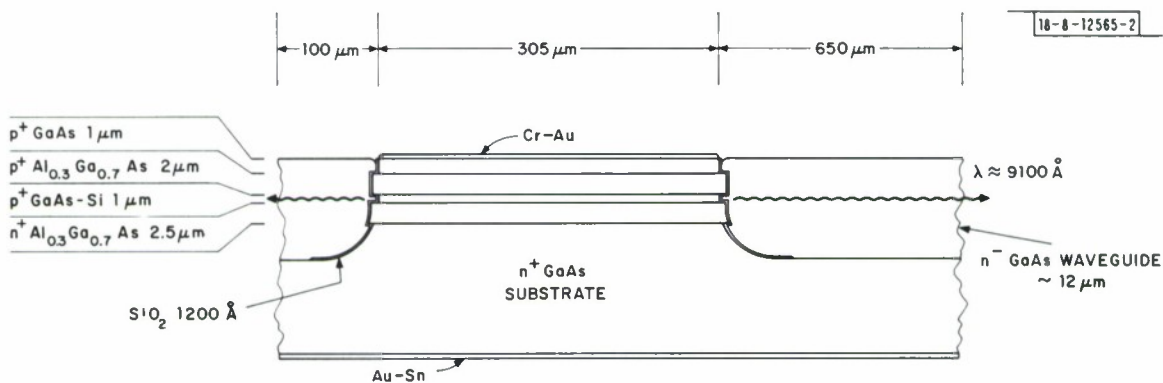


Fig. 3. Artist's representation of the cross section of a GaAs-AlGaAs DH laser integrated into a high-purity GaAs waveguide. Dimensions shown are typical. Typical laser widths were 45 and 90 μm .

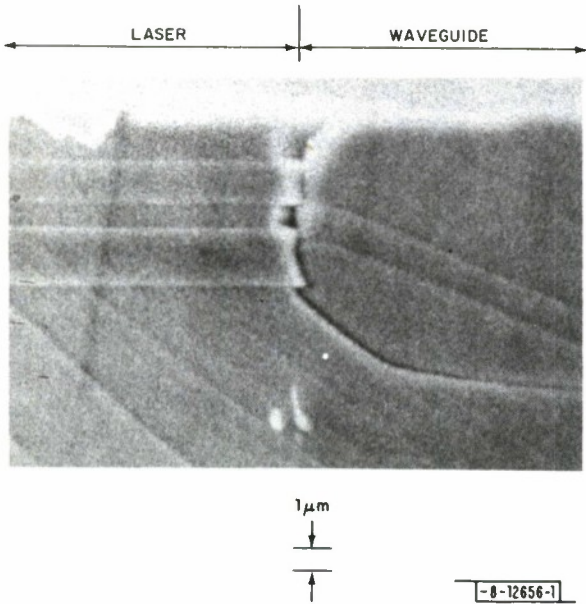


Fig. 4. Scanning electron micrograph of a cleaved cross section of the interface between the GaAs-AlGaAs DH laser and the high-purity GaAs waveguide. The GaAs has been selectively etched about $0.3 \mu\text{m}$ after cleaving to enhance details. Diagonal lines and slight chipping at the interface between the laser active region and waveguide are both due to imperfect cleaving (cleavage plane is 45° to plane of interface).

18-8-12655-1

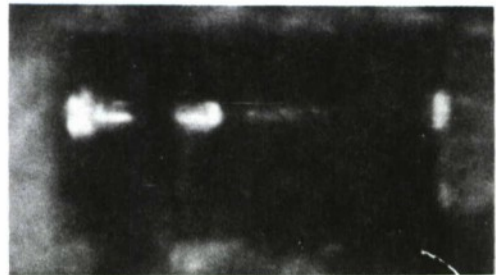
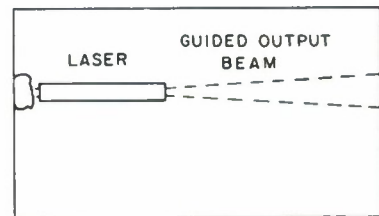


Fig. 5. Infrared photomicrograph and artist's sketch of top view of an operating integrated laser-waveguide structure. The laser itself is $45 \times 305 \mu\text{m}^2$. Brightness around the diode perimeter is exaggerated by the long exposure necessary to show up scattered light from the beam. Bright spot at left-hand edge is due to scattering of the beam by a large chip in the edge.



on a (100)-oriented substrate. The active region was doped heavily p-type with silicon in order to achieve laser emission near 9100 \AA for low loss in the GaAs waveguide. Using photolithographically defined pyrolytic SiO_2 as a mask, rectangular mesas $300 \text{ }\mu\text{m}$ long, 45 or $90 \text{ }\mu\text{m}$ wide, and 10 to $12 \text{ }\mu\text{m}$ high were created by chemically etching ($1 \text{ H}_2\text{SO}_4$; $8 \text{ H}_2\text{O}_2$; $1 \text{ H}_2\text{O}$ at 2°C) down through the grown layers to the substrate. Orientation of the rectangles along (100) directions resulted in mesas with walls perpendicular to the (100) wafer surface,¹⁵ the parallel end faces of the mesa then forming the end mirrors for the Fabry-Perot cavity. Etched and grown mesa Fabry-Perot homojunction lasers have been described earlier by Dobkin *et al.*¹⁶ and Blum *et al.*,¹⁷ respectively. After etching of the mesas, the superoxol etch described by Logan and Reinhart¹⁸ was used to selectively remove about $1 \text{ }\mu\text{m}$ of GaAs without etching the AlGaAs. This secondary etch appeared to improve the parallelism of end faces which had not etched perpendicular to the wafer surface during the formation of the mesas. However, the necessity or even the beneficial effect of this etch has not been established at present. In order to provide a reflecting dielectric mismatch between the end faces of the Fabry-Perot laser and the high-purity GaAs waveguide to be grown around the mesas, a layer of pyrolytic SiO_2 , 1200 to 1500 \AA thick, was deposited, photolithographically defined, and etched, leaving only the walls and tops of the mesas covered.* By vapor-phase epitaxy, the high-purity GaAs waveguide material was then grown on the substrate surrounding the mesas to a thickness approximately equal to the mesa height.

A scanning electron micrograph of a cross section of the laser-waveguide interface is shown in Fig. 4. It can be seen that the GaAs waveguide material makes intimate contact with the thin SiO_2 layer on the wall of the mesa. The apparent gap between the GaAs active region and the waveguide is the result of an imperfect cleave as well as the effect of the selective GaAs etch used after cleaving to enhance the definition of the various layers.

Contact to the tops of the mesas was made with sputtered Cr-Au, and an alloyed Au-Sn contact was made to the substrate. The wafer was then sawed into dice 0.45 mm wide by 1.0 mm long with the laser located near one end of the die. The lasers were pressure-contacted and tested using low-duty-cycle rectangular current pulses of 100-nsec duration. All measurements reported here were made with the devices at room temperature.

Above threshold, the laser radiation clearly was coupled into the waveguide and emitted from the waveguide layer at the end faces of the dice. An infrared photomicrograph of a top view of an operating laser-waveguide structure is shown in Fig. 5. The path of the beam is evident due to scattering of some radiation out of the waveguide by surface imperfections. The light leaking out around the perimeter of the diode appears much more intense than it actually is because of the long photographic exposure required to show the light scattered from the confined beam.

For diodes which appeared to exhibit the expected conventional two-mirror Fabry-Perot operation, the spacing of the observed spectral modes was about 3 \AA , which corresponds to the calculated separation of the longitudinal modes of the $300\text{-}\mu\text{m}$ -long mesa (assuming an effective refractive index of 4.5). The lowest measured threshold current density for these lasers was 7.5 kA/cm^2 for the $1\text{-}\mu\text{m}$ -thick active region. The measured external differential quantum

* A plane wave calculation of the transmission properties at 9100 \AA of a layer of SiO_2 sandwiched between GaAs gives a reflectivity of greater than 33 percent for a thickness t in the range $750 \text{ \AA} < t < 2375 \text{ \AA}$.

efficiencies of the laser-waveguide combination were somewhat low, about 3.5 percent. This may be the result of difficulties in collecting all the radiation emitted from the rough sawed end of the waveguide and/or the presence of internally reflected circulating modes¹⁹ which trap some of the energy within the laser. A rough measurement of the waveguide attenuation in these structures gave an upper limit of 8 cm^{-1} , a value which is higher than the 2 cm^{-1} of good high-purity GaAs waveguides¹⁰ at 9030 \AA , but not high enough to significantly affect the external quantum efficiency.

A number of the diodes fabricated were not so well behaved as those described above. The operation of most of these devices, particularly the wider ones, appeared to be dominated by total-internal-reflection modes. The observation of unusually low thresholds (as low as 3.5 kA/cm^2), low efficiencies (≤ 1 -percent external differential quantum efficiency), complex spectra, and emission from the corners of the mesas all are consistent with the presence of internally reflected modes.¹⁹ This is not too surprising since the etched side walls, as well as the ends of the lasers, were reflecting, and nothing was done to spoil the Q of the transverse cavity.

It is expected that considerable improvement in the performance of these integrated lasers can be obtained by the incorporation of a stripe-geometry structure to spoil the transverse Q and quench the internally circulating modes, as well as by reduction of the active region thickness to achieve lower threshold operation.

C. E. Hurwitz C. M. Wolfe
J. A. Rossi G. E. Stillman
J. J. Hsieh

II. LEAD-SALT INTEGRATED OPTICAL CIRCUITS:
LATTICE-MISFIT DISLOCATIONS IN HETEROEPITAXIAL $\text{Pb}_{1-x}\text{Sn}_x\text{Te}$

We have demonstrated using both molecular-beam and liquid-phase epitaxy (MBE and LPE) over three-orders-of-magnitude reduction in dislocation density in heteroepitaxial $\text{Pb}_{0.88}\text{Sn}_{0.12}\text{Te}$ layers grown on nearly lattice-matched $\text{PbTe}_{0.952}\text{Se}_{0.048}$ substrates with $\langle 100 \rangle$ orientation as opposed to PbTe substrates. The maximum theoretical dislocation density due to lattice mismatch for the 12-percent SnTe alloy on PbTe substrates is of the order of 10^9 cm^{-2} . Experimentally, we find the etch-pit density (EPD) for unmatched heteroepitaxy to be greater than 10^7 cm^{-2} with no obvious dependence on growth conditions or substrate preparation. For EPD much above 10^7 cm^{-2} , individual etch pits become impossible to resolve. This is the usual situation for unmatched epitaxy as shown in Fig. 6(a), where the entire surface of the epitaxial layer becomes uniformly gray in appearance after application of either Tilly's dislocation etch²⁰ or the low-voltage Norr electrolytic etch.²¹ Figure 6(b) shows the results of a dislocation etch on a lattice-matched epitaxial layer. Here, regions of high EPD are confined to areas of damage (due, in this case of LPE growth, to the slider which removes the melt). The EPD varies over the surface and is comparable to that of the substrate itself, in the range of 10^4 cm^{-2} .

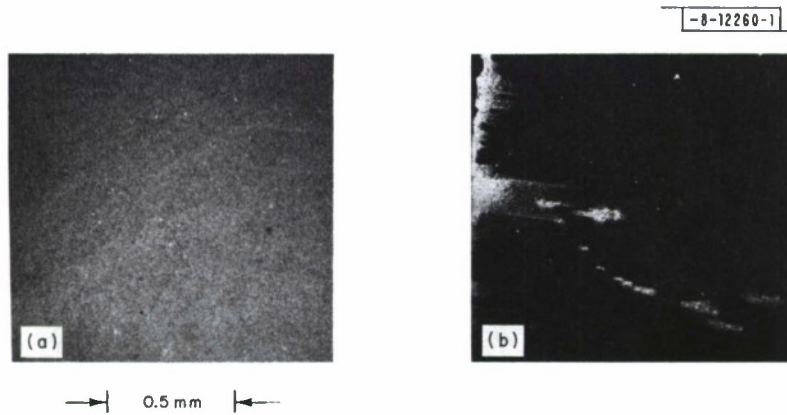


Fig. 6. Surfaces of epitaxial $\text{Pb}_{0.88}\text{Sn}_{0.12}\text{Te}$ after dislocation etch: (a) MBE layer on a PbTe substrate; EPD is essentially unresolved at any magnification and is uniform. (b) LPE layer on a $\text{PbTe}_{0.952}\text{Se}_{0.048}$ substrate; regions of high EPD are seen where damage occurs from the slider used to remove the melt.

Further studies of EPD using a variety of substrate-epitaxial-layer configurations bear out the general conclusion that sufficiently close lattice matching can be achieved between PbTeSe and PbSnTe alloys to significantly decrease misfit dislocations. These results are summarized in Table I. Here, the high EPD indicates $>10^7 \text{ cm}^{-2}$ and low EPD indicates on the order of 10^4 cm^{-2} or less, essentially determined by the substrate. It is interesting to note that no improvement in EPD was seen for $\text{Pb}_{0.88}\text{Sn}_{0.12}\text{Te}$ layers on $\text{Pb}_{0.90}\text{Sn}_{0.10}\text{Te}$ compared to PbTe substrates although the lattice mismatch $\Delta a/a$ is reduced from 2.4×10^{-3} to 6×10^{-4} . (Apparently, strain as small as 6×10^{-4} cannot be accommodated without plastic deformation.) We estimate that $\Delta a/a$ between $\text{Pb}_{0.88}\text{Sn}_{0.12}\text{Te}$ and $\text{PbTe}_{0.952}\text{Se}_{0.048}$ is less than 1×10^{-4} .

J. N. Walpole S. H. Groves
A. R. Calawa T. C. Harman

TABLE I
SUMMARY OF RESULTS

Epitaxial Layer	Substrate	Growth	EPD
$\text{Pb}_{0.88}\text{Sn}_{0.12}\text{Te}$	PbTe	LPE	High
$\text{Pb}_{0.88}\text{Sn}_{0.12}\text{Te}$	PbTe	MBE	High
PbTe	$\text{Pb}_{0.88}\text{Sn}_{0.12}\text{Te}$	MBE	High
$\text{Pb}_{0.88}\text{Sn}_{0.12}\text{Te}$	$\text{Pb}_{0.90}\text{Sn}_{0.10}\text{Te}$	LPE	High
PbTe	PbTe	MBE	Low
PbTe	PbTe	LPE	Low
$\text{Pb}_{0.88}\text{Sn}_{0.12}\text{Te}$	$\text{PbTe}_{0.952}\text{Se}_{0.048}$	MBE	Low
$\text{Pb}_{0.88}\text{Sn}_{0.12}\text{Te}$	$\text{PbTe}_{0.952}\text{Se}_{0.048}$	LPE	Low
$\text{PbTe}_{0.952}\text{Se}_{0.048}$	$\text{Pb}_{0.88}\text{Sn}_{0.12}\text{Te}$	MBE	Low
$\text{Pb}_{0.88}\text{Sn}_{0.12}\text{Te}$	$\text{Pb}_{0.88}\text{Sn}_{0.12}\text{Te}$	LPE	Low

REFERENCES

1. J. C. Tracy, W. Wiegman, R. A. Logan, and F. K. Reinhart, *Appl. Phys. Lett.* 22, 511 (1973).
2. F. A. Blum, D. W. Shaw, and W. C. Holton, *Appl. Phys. Lett.* 25, 116 (1974).
3. E. Garmire, H. Stoll, A. Yariv, and R. G. Hunsperger, *Appl. Phys. Lett.* 21, 87 (1972).
4. D. Redfield, *Phys. Rev.* 130, 916 (1963).
5. J. A. Rossi, S. R. Chinn, and H. Heckscher, *Appl. Phys. Lett.* 23, 25 (1973).
6. Y. Suematsu, M. Yamada, K. Hayashi, K. Furaya, and S. Ibukuro, 1974 IEEE International Laser Conference, Atlanta, Georgia, 18-20 November 1974; Y. Suematsu, M. Yamada, and K. Hayashi, *Proc. IEEE* 63, 208 (1975).
7. F. K. Reinhart and R. A. Logan, *Appl. Phys. Lett.* 25, 622 (1974).
8. D. R. Scifres, R. D. Burnham, and W. Streifer, *Appl. Phys. Lett.* 25, 203 (1974); D. B. Anderson, R. R. August, and J. E. Coker, *Appl. Opt.* 13, 2742 (1974); H. M. Stoll and D. H. Seib, *Appl. Opt.* 13, 1981 (1974); M. Nakamura, K. Aiki, Jun-ichi Umeda, A. Yariv, H. W. Yen, and T. Morikawa, *Appl. Phys. Lett.* 25, 487 (1974).
9. S. Wang, *IEEE J. Quantum Electron.* QE-10, 413 (1974).
10. G. E. Stillman, C. M. Wolfe, J. A. Rossi, and H. Heckscher, unpublished.
11. F. K. Reinhart, *Appl. Phys. Lett.* 22, 372 (1973).
12. J. C. Dymont, F. P. Kapron, and A. J. Springthorpe, Proc. 5th Intl. Symp. on GaAs and Related Compounds, Deauville, 1974 (Inst. of Phys., London, to be published).
13. G. E. Stillman, C. M. Wolfe, J. A. Rossi, and J. P. Donnelly, *Appl. Phys. Lett.* 25, 671 (1974).
14. G. E. Stillman, C. M. Wolfe, A. G. Foyt, and W. T. Lindley, *Appl. Phys. Lett.* 24, 8 (1974).
15. Y. Tarui, Y. Komiya, and Y. Harada, *J. Electrochem. Soc.* 118, 118 (1971).
16. A. S. Dobkin, V. V. Kokorev, G. A. Lapitskaya, A. A. Pleshov, O. N. Prozorov, L. A. Rivkin, G. A. Sukharev, V. S. Shil'dyaev, and S. D. Yakubovich, *Sov. Phys. -Semiconductors* 4, 515 (1970).
17. F. A. Blum, K. L. Lawley, F. H. Doerbeck, and W. C. Holton, *Appl. Phys. Lett.* 25, 620 (1974).
18. R. A. Logan and F. K. Reinhart, *J. Appl. Phys.* 44, 4172 (1973).
19. I. Hayashi and M. B. Panish, *J. Appl. Phys.* 41, 150 (1970).
20. G. P. Tilly, *Br. J. Appl. Phys.* 12, 524 (1961).
21. M. K. Norr, *J. Electrochem. Soc.* 109, 433 (1962).

REPORT DOCUMENTATION PAGE		READ INSTRUCTIONS BEFORE COMPLETING FORM
1. REPORT NUMBER ESD-TR-75-183	2. GOVT ACCESSION NO.	3. RECIPIENT'S CATALOG NUMBER
4. TITLE (and Subtitle) Integrated Optical Circuits		5. TYPE OF REPORT & PERIOD COVERED Semiannual Technical Summary 1 July - 31 December 1974
		6. PERFORMING ORG. REPORT NUMBER
7. AUTHOR(s) Melngailis, Ivars		8. CONTRACT OR GRANT NUMBER(s) F19628-73-C-0002
9. PERFORMING ORGANIZATION NAME AND ADDRESS Lincoln Laboratory, M.I.T. P.O. Box 73 Lexington, MA 02173		10. PROGRAM ELEMENT, PROJECT, TASK AREA & WORK UNIT NUMBERS ARPA Order 2074 Program Element 61101E
11. CONTROLLING OFFICE NAME AND ADDRESS Advanced Research Projects Agency 1400 Wilson Boulevard Arlington, VA 22209		12. REPORT DATE 31 December 1974
		13. NUMBER OF PAGES 16
14. MONITORING AGENCY NAME & ADDRESS (if different from Controlling Office) Air Force Cambridge Research Laboratories Hanscom AFB Bedford, MA 01731		15. SECURITY CLASS. (of this report) Unclassified
		15a. DECLASSIFICATION DOWNGRADING SCHEDULE
16. DISTRIBUTION STATEMENT (of this Report) Approved for public release; distribution unlimited.		
17. DISTRIBUTION STATEMENT (of the abstract entered in Block 20, if different from Report)		
18. SUPPLEMENTARY NOTES None		
19. KEY WORDS (Continue on reverse side if necessary and identify by block number)		
Integrated Optical Circuits electroabsorption effect GaAs epitaxial growth	heterodyne detection avalanche photodiodes acoustic waves Schottky barrier	proton bombardment Hg _{1-x} Cd _x Te-CdTe Pb _{1-x} Sn _x Te
20. ABSTRACT (Continue on reverse side if necessary and identify by block number)		
<p>Detailed measurements of the attenuation of high-purity GaAs waveguides have been made for wavelengths from 0.90 to 1.06 μm. Fabry-Perot GaAs-AlGaAs double-heterostructure lasers have been integrated into these low-loss GaAs waveguides and appear attractive as sources for monolithic GaAs-based integrated optical circuits.</p> <p>Large reductions of lattice-misfit dislocation densities in heteroepitaxial Pb_xSn_{1-x}Te layers have been achieved by growth on nearly lattice-matched substrates.</p>		